Draft version July 1, 2020
Typeset using LaTeX **preprint** style in AASTeX62

Constraining M_ν with the Bispectrum II: the Information Content of the Galaxy Bispectrum

ChangHoon Hahn,[1,2,*] Francisco Villaescusa-Navarro,[3,4] and ...

[1] *Lawrence Berkeley National Laboratory, 1 Cyclotron Rd, Berkeley CA 94720, USA*
[2] *Berkeley Center for Cosmological Physics, University of California, Berkeley, CA 94720, USA*
[3] *Center for Computational Astrophysics, Flatiron Institute, 162 5th Avenue, New York, NY 10010, USA*
[4] *Department of Astrophysical Sciences, Princeton University, Peyton Hall, Princeton NJ 08544, USA*

(Dated: `DRAFT --- d642f47 --- 2020-06-25 --- NOT READY FOR DISTRIBUTION`)

ABSTRACT

Massive neutrinos suppress the growth of structure below their free-streaming scale and leave an imprint on large-scale structure that can be measured to constrain their total mass, M_ν. With the standard analysis of two-point clustering stastics, M_ν constraints are severely limited by parameter degeneracies. Hahn et al. (2020) demonstrated that the halo bispectrum, the next higher-order statistic, can break these degeneracies and dramatically improve constraints on M_ν and other cosmological parameters. In this paper, we present the advantages of analyzing the redshift-space *galaxy* bispectrum. We construct 195,000 mock galaxy catalogs from the Quijote suite of N-body simulations with the halo occupation distribution (HOD) model, which provides an effective galaxy bias framework well-suited for simulation-based approaches. Using these mocks, we present the Fisher matrix forecasts of $\{\Omega_{\rm m}, \Omega_{\rm b}, h, n_s, \sigma_8, M_\nu\}$ and quantify for the first time, the total information content of the redshift-space galaxy bispectrum down to nonlinear scales. For $k_{\rm max} = 0.5\,h/{\rm Mpc}$, with the galaxy bispectrum, constraints on $\Omega_{\rm m}$, $\Omega_{\rm b}$, h, n_s, σ_8 improve by **CH:** 3.3, 3.6, 4.5, 4.9, and 4.7 over power spectrum constraints, even after marginalizing over HOD parameters. For M_ν, we derive 5.6× tighter constraints with the bispectrum. Including priors from *Planck* , the bispectrum improves cosmological constraints by **CH:** $\gtrsim 2\times$. While effects such as survey geometry and assembly bias will impact the constraining power for galaxy surveys, these constraints are derived for $(1\ h^{-1}{\rm Gpc})^3$, a substantially smaller volume than upcoming surveys. Therefore, we conclude that including the galaxy bispectrum will significantly improve cosmological constraints, especially M_ν, for upcoming galaxy surveys.

Keywords: cosmology: cosmological parameters — cosmology: large-scale structure of Universe. — cosmology: theory

1. INTRODUCTION

TODO

* hahn.changhoon@gmail.com

Neutrino mass background (condensed version of paper 1) The discovery of the lower bound on the sum of neutrino masses ($M_\nu \gtrsim 0.06$ eV), provides conclusive evidence of physics beyond the Standard Model of particle physics (**??**). A more precise measurement of M_ν has the potential to distinguish between the 'normal' and 'inverted' neutrino mass hierarchy scenarios and further reveal the physics of neutrinos. However, neutrino oscillation experiments, which are insensitive to M_ν, and other upcoming laboratory experiments (*e.g.* double beta decay and tritium beta decay) are not sufficient to distinguish between the mass hierarches (**??**). Through the cosmic neutrino background, neutrinos affect the expansion history and the growth of cosmic structure. Measuring these effects provides complementary and potentially more precise measurements of M_ν.

Neutrinos, in the early Universe, are relativistic and contribute to the energy density of radiation. Later as they become non-relativistic, they contribute to the energy density of matter. This transition affects the expansion history of the Universe and leaves imprints observable in the cosmic microwave background (CMB) anisotropy spectrum (**??**). Massive neutrinos also impact the growth of structure. On large scales, neutrino perturbations are indistinguishable from perturbations of cold dark matter (CDM). However, on scales smaller than their free-streaming scale, neutrinos do not contribute to the clustering and thereby reduce the amplitude of the total matter power spectrum. In addition, they also reduce the growth rate of CDM perturbations at late times. This combined suppression of the small-scale matter power spectrum leaves measurable imprints on the CMB as well as large-scale structure. For more on details the effect of neutrinos in cosmological observables, we refer readers to **??** and **?**.

transition to why LSS neutrino mass measurement is important (condensed version of paper 1) TODO

The tightest cosmological constraints on M_ν currently come from combining CMB data with other cosmological probes. Temperature and large angle polarization data from the *Planck* satellite places an upper bound of $M_\nu < 0.54$ eV with 95% confidence level (**?**). Adding the Baryon Acoustic Oscillation (BAO) to the *Planck* likelihood breaks geometrical degeneracies (among M_ν, h, $\Omega_{\rm m}$) and significantly tightens the upper bound to $M_\nu < 0.16$ eV. CMB lensing further tightens the bound to $M_\nu < 0.13$ eV, though not as significantly. Future improvements will likely continue to come from combining CMB data on large scales with clustering/lensing data on small scales and low redshifts, where the suppression of power by neutrinos is strongest (**?**). CMB experiments, however, measure the combined quantity $A_s e^{-2\tau}$, where τ is the optical depth of reionization. Hence, improvements in neutrino mass constraints obtained from comparing the power spectrum on small and large scales will heavily rely on a better determination of τ (**???**). The best constraints on τ currently come from *Planck* — $\tau = 0.054 \pm 0.007$. However, most upcoming ground-based CMB experiments (*e.g.* CMB-S4) will not observe scales larger than $\ell < 30$, and therefore will not directly constrain τ (**?**). While the upcoming CLASS experiment aims to improve τ constraints (**?**), proposed future space-based experiments such as LiteBIRD[1] and LiteCOrE[2], which have the greatest potential to precisely measure τ, have yet to be confirmed. CMB data, however, is not the only way to improve M_ν constraints. The imprint of neutrinos on 3D clustering of galaxies can be measured to constrain M_ν and with the sheer cosmic

[1] http://litebird.jp/eng/
[2] http://www.core-mission.org/

volumes mapped, upcoming surveys such as DESI[3], PFS[4], EUCLID[5], and WFIRST[6] will be able tightly constrain M_ν (?????).

why the bispectrum: condensed version of paper1 TODO

A major limitation of using 3D clustering is obtaining accurate theoretical predictions beyond linear scales, for bias tracers, and in redshift space. Simulations have made huge strides in accurately and efficiently modeling nonlinear structure formation with massive neutrinos (*e.g.* Brandbyge et al. 2008; ?; ?; ?; ?; ?). In conjunction, new simulation based 'emulation' models that exploit the accuracy of N-body simulations while minimizing the computing budget have been applied to analyze small-scale galaxy clustering with remarkable success (*e.g.* ???McClintock et al. 2018; ?; ?). Developments on these fronts have the potential to unlock the information content in nonlinear clustering to constrain M_ν.

Various works have examined the impact of neutrino masses on nonlinear clustering of matter in real-space (*e.g.* Brandbyge et al. 2008; ?; ?; ?; Viel et al. 2010; ?; ?; ?; ?) and in redshift-space (???). Most recently, using a suite of more than 1000 simulations, ? examined the impact of M_ν on the redshift-space matter and halo power spectrum to find that the imprint of M_ν and σ_8 on the power spectrum are degenerate and differ by $< 1\%$ (see also Figure ??). The strong $M_\nu - \sigma_8$ degeneracy poses a serious limitation on constraining M_ν with the power spectrum. However, information in the nonlinear regime cascades from the power spectrum to higher-order statistics — *e.g.* the bispectrum. In fact, the bispectrum has a comparable signal-to-noise ratio to the power spectrum on nonlinear scales (Sefusatti & Scoccimarro 2005; ?). summary of paper 1 results TODO

paragraph on others including galaxy bias for M_ν constraints, but they're all in the perturbation theory framework so none extend to nonlinear scales. In this paper we include galaxy bias in a simulation-based approach with emulation and LFI in mind. We use HODs, which are (a sentence on hods)

Furthermore, although M_ν is not included in their analyses, Sefusatti et al. (2006) and Yankelevich & Porciani (2019) have shown that including the bispectrum significantly improves constraints on cosmological parameters. Including M_ν, Chudaykin & Ivanov (2019) find that the bispectrum significantly improves constraints for M_ν. Their forecasts, however, do not include the constraining power on nonlinear scales (Section ??). No work to date has quantified the total information content and constraining power of the full redshift-space bispectrum down to nonlinear scales — especially for M_ν.

2. THE QUIJOTE SIMULATION SUITE

We use a subset of simulations from the Quijote suite, a set of over 43,000 N-body simulations that spans over 7000 cosmological models and contains, at a single redshift, over 8.5 trillion particles (Villaescusa-Navarro et al. 2019). The Quijote suite was designed to quantify the information content of cosmological observables and also to train machine learning algorithms. Hence, the suite includes enough realizations to accurately estimate the covariance matrices of high-dimensional observables such as the bispectrum as well as the derivatives of these observables with respect to cosmological

[3] https://www.desi.lbl.gov/
[4] https://pfs.ipmu.jp/
[5] http://sci.esa.int/euclid/
[6] https://wfirst.gsfc.nasa.gov/

Table 1. The Quijote suite includes 15,000 standard N-body simulations at the fiducial cosmology to accurately estimate the covariance matrices. It also includes sets of 500 simulations at 13 other cosmologies, where only one parameter is varied from the fiducial value (underlined), to estimate derivatives of observables along the cosmological parameters.

Name	M_ν	Ω_m	Ω_b	h	n_s	σ_8	ICs	realizations
Fiducial	0.0	0.3175	0.049	0.6711	0.9624	0.834	2LPT	15,000
Fiducial ZA	0.0	0.3175	0.049	0.6711	0.9624	0.834	Zel'dovich	500
M_ν^+	0.1 eV	0.3175	0.049	0.6711	0.9624	0.834	Zel'dovich	500
M_ν^{++}	0.2 eV	0.3175	0.049	0.6711	0.9624	0.834	Zel'dovich	500
M_ν^{+++}	0.4 eV	0.3175	0.049	0.6711	0.9624	0.834	Zel'dovich	500
Ω_m^+	0.0	0.3275	0.049	0.6711	0.9624	0.834	2LPT	500
Ω_m^-	0.0	0.3075	0.049	0.6711	0.9624	0.834	2LPT	500
Ω_b^+	0.0	0.3175	0.051	0.6711	0.9624	0.834	2LPT	500
Ω_b^-	0.0	0.3175	0.047	0.6711	0.9624	0.834	2LPT	500
h^+	0.0	0.3175	0.049	0.6911	0.9624	0.834	2LPT	500
h^-	0.0	0.3175	0.049	0.6511	0.9624	0.834	2LPT	500
n_s^+	0.0	0.3175	0.049	0.6711	0.9824	0.834	2LPT	500
n_s^-	0.0	0.3175	0.049	0.6711	0.9424	0.834	2LPT	500
σ_8^+	0.0	0.3175	0.049	0.6711	0.9624	0.849	2LPT	500
σ_8^-	0.0	0.3175	0.049	0.6711	0.9624	0.819	2LPT	500

parameters. For the derivatives, the suite includes sets of simulations run at different cosmologies where only one parameter is varied from the fiducial cosmology: $\Omega_{\rm m}$=0.3175, $\Omega_{\rm b}$=0.049, h=0.6711, n_s=0.9624, σ_8=0.834, and M_ν=0.0 eV. Along $\Omega_{\rm m}$, $\Omega_{\rm b}$, h, n_s, and σ_8, the fiducial cosmology is adjusted by either a small step above or below the fiducial value: $\{\Omega_{\rm m}^+, \Omega_{\rm m}^-, \Omega_{\rm b}^+, \Omega_{\rm b}^-, h^+, h^-, n_s^+, n_s^-, \sigma_8^+, \sigma_8^-\}$. Along M_ν, because $M_\nu \geq 0.0$ eV and the derivative of certain observable with respect to M_ν is noisy, Quijote includes sets of simulations for $\{M_\nu^+, M_\nu^{++}, M_\nu^{+++}\} = \{0.1, 0.2, 0.4\}$ eV. See Table 1 for a summary of the Quijote simulations used in this work.

The initial conditions for all the simulations were generated at $z = 127$ using second-order perturbation theory for simulations with massless neutrinos ($M_\nu = 0.0$ eV) and the Zel'dovich approximation for massive neutrinos ($M_\nu > 0.0$ eV). The initial conditions with massive neutrinos take their scale-dependent growth factors/rates into account using the Zennaro et al. (2017) method, while for the massless neutrino case we use the traditional scale-independent rescaling. From the initial conditions, the simulations follow the gravitational evolution of 512^3 dark matter particles, and 512^3 neutrino particles for massive neutrino models, to $z = 0$ using Gadget-III TreePM+SPH code (Springel 2005). Simulations with massive neutrinos are run using the "particle method", where neutrinos are described as a collisionless and pressureless fluid and therefore modeled as particles, same as CDM (Brandbyge et al. 2008; Viel et al. 2010). Halos are identified using the Friends-

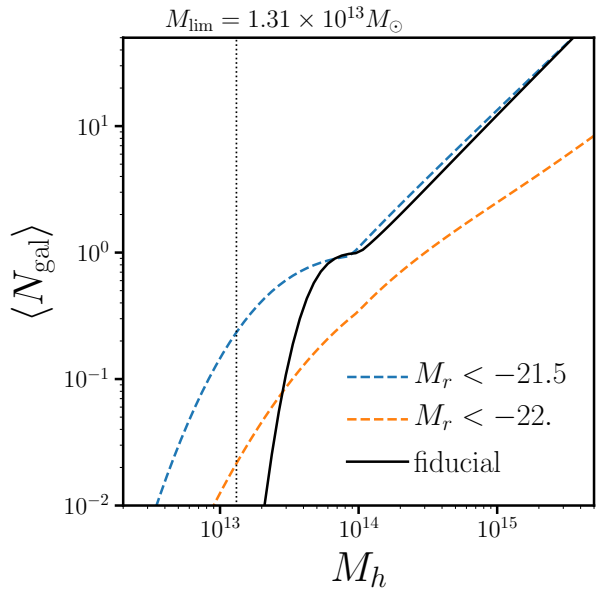

Figure 1. Our fiducial halo occupation (black) parameterized using the standard Zheng et al. (2007) HOD model. We derive the parameter values of our fiducial HOD model (Eq. 4) by modifying the best-fit HOD parameters of the SDSS $M_r < -21.5$ and $< -22.$ samples from Zheng et al. (2007) to accommodate the $M_{\rm lim} = 3.2 \times 10^{13} h^{-1} M_\odot$ halo mass limit of the QUIJOTE simulations (black dashed). We include the best-fit halo occupations of the SDSS $M_r < -21.5$ (blue dashed) and $< -22.$ samples (orange dashed) from Zheng et al. (2007) for reference. Our fiducial HOD sample has a galaxy number density of $\overline{n}_g \sim 1.63 \times 10^{-4}\ h^3/{\rm Mpc}^3$.

of-Friends algorithm (FoF; Davis et al. 1985) with linking length $b = 0.2$ on the CDM + baryon distribution. We limit the halo catalogs to halos with masses above $M_{\rm lim} = 3.2 \times 10^{13} h^{-1} M_\odot$. For the fiducial cosmology, the halo catalogs have $\sim$156,000 halos ($\bar{n}_h \sim 1.56 \times 10^{-4}\ h^3{\rm Gpc}^{-3}$) with $\bar{n} P_0(k = 0.1) \sim 3.23$. We refer readers to Villaescusa-Navarro et al. (2019) and Hahn et al. (2019) for further details on the QUIJOTE simulations.

3. HALO OCCUPATION DISTRIBUTION

We are interested in quantifying the information content of the galaxy bispectrum. For a perturbation theory approach, this involves incorporating a bias model for galaxies (*e.g.* Sefusatti et al. 2006; Yankelevich & Porciani 2019; Chudaykin & Ivanov 2019). Perturbation theory approaches, however, break down on small scales and limit the constraining power from nonlinear regime. Instead, in our simulation based approach we use the halo occupation distribution (HOD) framework (*e.g.* Zheng et al. 2005; Leauthaud et al. 2012; Tinker et al. 2013; Zentner et al. 2016; Vakili & Hahn 2019).HOD models statistically populate galaxies in dark matter halos by specifying the probability of a given halo hosting a certain number of galaxies. This statistical prescription for connecting galaxies to halos has been remarkably successful in reproducing the observational statistics of galaxies (*e.g.* galaxy clustering) and, as a result, is the standard approach for constructing simulated galaxy mock catalogs in galaxy clustering analyses to estimate covariance matrices and test systematic effects (*e.g.*

Rodríguez-Torres et al. 2016, 2017; Beutler et al. 2017). More importantly, HOD models in simulations for build galaxy clustering emulators (see the Aemulus project McClintock et al. 2018; **?**). Emulation, as we mention above, is one of the most promising approaches for modeling small scale galaxy clustering and is what we're trying to forecast in this work.

In the simplest HOD models, the probability of a given halo hosting N galaxies of a certain class is dictated by its halo mass — $P(N|M_h)$.We use the standard $P(N|M_h)$ model from Zheng et al. (2007), which has been ubiquitously used in galaxy clustering analyses (*e.g.* Sinha et al. 2018, many more). The model specifies the mean number of galaxies in a halo as TODO

$$\langle N_{\rm gal} \rangle = \langle N_{\rm cen} \rangle + \langle N_{\rm sat} \rangle \tag{1}$$

with mean central galaxy occupation

$$\langle N_{\rm cen} \rangle = \frac{1}{2}\left[1 + {\rm erf}\left(\frac{\log M_h - \log M_{\rm min}}{\sigma_{\log M}}\right)\right] \tag{2}$$

and mean satellite galaxy occupation

$$\langle N_{\rm sat} \rangle = \langle N_{\rm cen} \rangle \left(\frac{M_h - M_0}{M_1}\right)^{\alpha}. \tag{3}$$

The mean number of centrals in a halo transitions smoothly from 0 to 1 for halos with mass $M_h > M_{\rm min}$. The width of the transition is dictated by $\sigma_{\log M}$, which reflects the scatter between stellar mass/luminosity and halo mass (**?**). For $M_h > M_{\rm min}$, $\langle N_{\rm sat} \rangle$ follows a power law with slope α. M_0 is the halo mass cut-off for satellite occupation and $M_h = M_0 + M_1$ is the typical mass scale for halos to host one satellite galaxy. The numbers of centrals and satellites for each halo are drawn from Bernoulli and Poisson distribution, respectively. Central galaxies are placed at the center of the halo while position and velocity of the satellite galaxies are sampled from a Navarro et al. (1997) (NFW) profile.

The halo occupation in the Zheng et al. (2007) model depends soley on M_h. Simulations, however, find evidence that secondary halo properties such as concentration or formation history correlate with spatial distribution of halos — a phenomenon referred to as "halo assembly bias" (*e.g.* Sheth & Tormen 2004; Gao et al. 2005; Harker et al. 2006; Wechsler et al. 2006; Dalal et al. 2008; Wang et al. 2009; Lacerna et al. 2014; Contreras et al. 2020; Hadzhiyska et al. 2020). A model that only depends on M_h, does not account for this halo assembly bias and may not sufficient describe the connection between galaxies and halos. Moreover, if unaccounted for in the HOD model, and thus not marginalized over, halo assembly bias may impact the cosmological parameter constraints. However, for the high luminosity samples in SDSS ($M_r < -21.5$ and < -21), Zentner et al. (2016) and Vakili & Hahn (2019) find little evidence for assembly bias in the galaxy clustering. Beltz-Mohrmann et al. (2020) also find that a basi HOD is sufficent to reproduce galaxy clustering of high luminosity galaxies in hydrodynamic simulations. Therefore, in this work we use the standard Zheng et al. (2007) HOD model to model the galaxy–halo connection.

For the fiducial parameter values of the HOD model we used values motivated by best-fit HOD parameters from the literature, namely the Zheng et al. (2007) fits to the SDSS $M_r < -21.5$ and -22 samples:

$$\{M_{\rm min}, \sigma_{\log M}, \log M_0, \alpha, \log M_1\} = \{13.65, 0.2, 14., 1.1, 14.\}. \quad (4)$$

In Figure 1 we present the halo occupation of our fiducial HOD parameters (black). We include the best-fit halo occupations of the SDSS $M_r < -21.5$ (blue) and -22 (orange) samples from Zheng et al. (2007) for comparison. We also mark the halo mass limit, $M_{\rm lim}$, of the Quijote simulations (black dotted). At $M_h \sim 10^{13} M_\odot$, the best-fit halo occupations of the SDSS samples extend below $M_{\rm lim}$ — *i.e.* they have halos below $M_{\rm lim}$ that host galaxies. This prevents us from directly using the values from the literature and instead, we reduce $\sigma_{\log M}$ to 0.2 dex. We confirm using Quijote simulations with higher mass resolution (1024^3 CDM particles) that $M_{\rm lim}$ does not impact the observables or their derivatives in our analysis for our fiducial HOD parameters.

As we mention above, $\sigma_{\log M}$ reflects the scatter between stellar mass/luminosity and halo mass. The high $\sigma_{\log M}$ in the $M_r < -21.5$ and -22 SDSS samples is caused by the turnover in this relation at high stellar mass/luminosity. Our fiducial halo occupation, with its lower $\sigma_{\log M}$, results in a galaxy sample with a tighter scatter than the samples selected based on M_r or M_* cuts, *e.g.* used in SDSS and BOSS. Hence, such a sample would require selecting based on observable galaxy properties that correlate more strong with M_h than luminosity or M_*. While there is some evdience that such observables are availabe (*e.g.* $L_{\rm sat}$; Alpaslan & Tinker 2019), they have not been adopted for selecting galaxy samples. Regardless, in this work we focus on quantifying the information content of the galaxy bispectrum and not on analyzing an observed galaxy sample. We therefore opt for a more conservative set of HOD parameters with respect to $M_{\rm lim}$. For our fiducial halo occupation at the fiducial cosmology, the galaxy catalog has $\bar{n}_g \sim 1.63 \times 10^{-4}\ h^3{\rm Gpc}^{-3}$ and linear bias of $b_g \sim 2.55$.

We construct galaxy catalogs using 22,000 N-body simulations of the Quijote suite: 15,000 at the fiducial cosmology and 500 at the 14 other cosmologies listed in Table 1 of **?**. We use the fiducial HOD parameters for these catalogs. In addition, we construct galaxy catalogs from 500 N-body simulations at the fiducial cosmology using 10 additional sets of HOD parameters. We use these catalogs to estimate the derivatives of our observables with respect to the 5 HOD parameters — a pair per parameter. For each pair we vary one HOD paramter above and below the fiducial value by step sizes:

$$\{\Delta M_{\rm min}, \Delta\sigma_{\log M}, \Delta \log M_0, \Delta\alpha, \Delta \log M_1\} = \{0.05, 0.2, 0.2, 0.2, 0.2\}. \quad (5)$$

We generate one set of HOD realizations for the galaxy catalogs used to estimate the covariance matrices (fiducial cosmology and HOD) and apply redshift-space distortions along the z-axis. We generate 5 sets of HOD realizations for the galaxy catalogs used to estimate the derivatives and use apply redshift-space distortions along all 3 directions. All galaxy catalogs constructed for this paper are publicly available at where to access the galaxy catalogs. *In total, we use 195,000 galaxy catalogs in our analysis.* TODO

4. BISPECTRUM AND COSMOLOGICAL PARAMETER FORECASTS

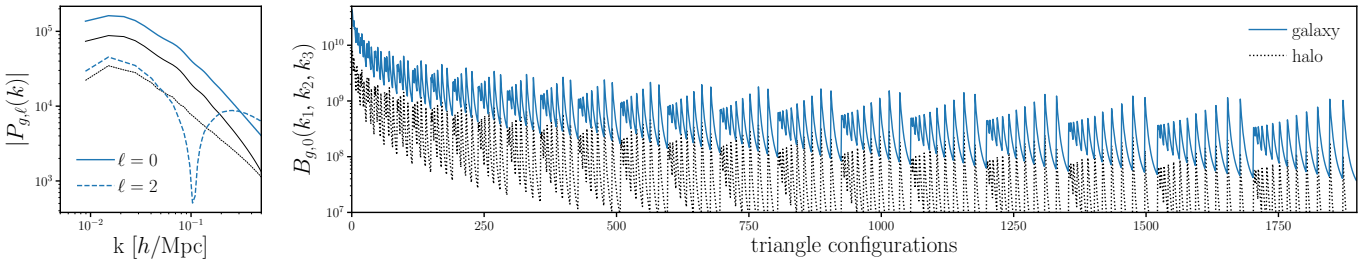

Figure 2. The redshift-space galaxy power spectrum multipoles (P_ℓ^g; left) and bispectrum monopole (B_0^g; right) of the galaxy catalog at the fiducial cosmology, constructed using the fiducial HOD parameters (blue). The P_ℓ^g and B_0^g are averaged over 15,000 N-body realizations and measured using the same FFT-based estimator as Hahn et al. (2020). In the left panel, we plot both the P_ℓ^g monopole ($\ell = 0$; solid) and quadrupole ($\ell = 2$; dashed). In the right panel, we plot B_0^g for all 1898 triangle configurations with $k_1, k_2, k_3 \geq k_{\rm max} = 0.5\,h/{\rm Mpc}$. The configurations are ordered by looping through k_3 in the inner most loop and k_1 in the outer most loop satisfying $k_1 \leq k_2 \leq k3$. We include for comparison the Hahn et al. (2020) halo P_ℓ^h and B_0^h at the fiducial cosmology (black). We note that the fiducial galaxy catalog has $\bar{n}_g \sim 1.63 \times 10^{-4}\ h^3{\rm Gpc}^{-3}$ and linear bias of $b_g \sim 2.55$.

We measure the bispectrum and parameter forecasts using the same methods as Hahn et al. (2020). For further details, we therefore refer readers to Hahn et al. (2020).

To measure B_0^g, we use a Fast Fourier Transform (FFT) based estimator similar to the ones described in Sefusatti & Scoccimarro (2005), Scoccimarro (2015), and Sefusatti et al. (2016). Galaxy positions are first interpolated onto a grid, $\delta(\boldsymbol{x})$, using a fourth-order interpolation scheme, which has advantageous anti-aliasing properties that allow unbiased measurements up to the Nyquist frequency (Hockney & Eastwood 1981; Sefusatti et al. 2016). After Fourier transforming $\delta(\boldsymbol{x})$ to get $\delta(\boldsymbol{k})$, we measure the bispectrum monopole:

$$B_0^g(k_1, k_2, k_3) = \frac{1}{V_B} \int_{k_1} {\rm d}^3q_1 \int_{k_2} {\rm d}^3q_2 \int_{k_3} {\rm d}^3q_3\ \delta_{\rm D}(\boldsymbol{q}_{123})\ \delta(\boldsymbol{q}_1)\ \delta(\boldsymbol{q}_2)\ \delta(\boldsymbol{q}_3) - B_0^{\rm SN}. \tag{6}$$

δ_D is the Dirac delta function, V_B is the normalization factor proportional to the number of triplets that can be found in the k_1, k_2, k_3 triangle bin, and $B_0^{\rm SN}$ is the correction term for the Poisson shot noise. Throughout the paper, we use $\delta(\boldsymbol{x})$ grids with $N_{\rm grid} = 360$ and triangle configurations defined by k_1, k_2, k_3 bins of width $\Delta k = 3k_f = 0.01885\,h/{\rm Mpc}$, where $k_f = 2\pi/(1000\ h^{-1}{\rm Mpc})$.

In Figure 2, we present the redshift-space galaxy power spectrum multipoles (P_ℓ^g; left) and bispectrum (B_0^g; right) of the galaxy catalog at the fiducial cosmology, constructed using the fiducial HOD parameters (blue). The P_ℓ^g and B_0^g are averaged over 15,000 N-body realizations. In the left panel, we plot both the power spectrum monopole ($\ell = 0$; solid) and quadrupole ($\ell = 2$; dashed). In the right panel, we plot B_0^g for all 1898 triangle configurations with $k_1, k_2, k_3 \geq k_{\rm max} = 0.5\,h/{\rm Mpc}$. The configurations are ordered by looping through k_3 in the inner most loop and k_1 in the outer most loop satisfying $k_1 \leq k_2 \leq k3$. For comparison, we include the redshift-space halo power spectrum and bispectrum at the fiducial cosmology from Hahn et al. (2020) (black).

To estimate the constraining power of B_0^g, we use Fisher information matrices, which have been ubiquitously used in cosmology (*e.g.* Jungman et al. 1996; Tegmark et al. 1997; Dodelson 2003; Heavens 2009; Verde 2010):

$$F_{ij} = -\left\langle \frac{\partial^2 \ln \mathcal{L}}{\partial\theta_i \partial\theta_j} \right\rangle, \tag{7}$$

As in Hahn et al. (2020), we assume that the B_0^g lieklihood is Gaussian and neglect the covariance derivative term (Carron 2013) and estimate the Fisher matrix as

$$F_{ij} = \frac{1}{2}\,\mathrm{Tr}\left[\boldsymbol{C}^{-1}\left(\frac{\partial B_0^g}{\partial\theta_i}\frac{\partial B_0^{g\,T}}{\partial\theta_j} + \frac{\partial B_0^{g\,T}}{\partial\theta_i}\frac{\partial B_0^g}{\partial\theta_j}\right)\right]. \tag{8}$$

We derive the covariance matrix, $\boldsymbol{C}$, using the 15,000 galaxy catalogs at the fiducial cosmology. The derivatives along the cosmological and HOD parameters, $\partial B_0^g/\partial\theta_i$, are estimated using finite difference. For all parameters besides M_ν, we estimate

$$\frac{\partial B_0^g}{\partial\theta_i} \approx \frac{B_0^g(\theta_i^+) - B_0^g(\theta_i^-)}{\theta_i^+ - \theta_i^-}, \tag{9}$$

where $B_0^g(\theta_i^+)$ and $B_0^g(\theta_i^-)$ are the average bispectrum of the 7,500 realizations at θ_i^+ and θ_i^-, the HOD + cosmological parameter values above and below the fiducial parameters. For M_ν, where the fiducial value is 0.0 eV, we use the galaxy catalogs at M_ν^+, M_ν^{++}, $M_\nu^{+++} = 0.1, 0.2, 0.4$ eV (Table 1) to estimate

$$\frac{\partial B_0^g}{\partial M_\nu} \approx \frac{-21B_0^g(\theta_{\rm fid}^{\rm ZA}) + 32B_0^g(M_\nu^+) - 12B_0^g(M_\nu^{++}) + B_0^g(M_\nu^{+++})}{1.2}, \tag{10}$$

which provides a $\mathcal{O}(\delta M_\nu^2)$ order approximation. Since the simulations at M_ν^+, M_ν^{++}, and M_ν^{+++} are generated from Zel'dovich initial conditions, we use simulations at the fiducial cosmology also generated from Zel'dovich initial conditions ($\theta_{\rm fid}^{\rm ZA}$). We emphasize that by using galaxy catalogs constructed from N-body simulations, we are able to accurately extend our analysis beyond the limitations of analytic methods (*e.g.* perturbation theory) down to the nonlinear regime.

5. RESULTS

We present the Fisher matrix constraints for M_ν and other cosmological parameters from the redshift-space galaxy P_ℓ^g (blue), B_0^g (green), and combined $P_\ell^g + B_0^g$ (orange) in Figure 3. These constraints marginalize over the Zheng et al. (2007) HOD parameters (bottom panels) and extends to $k_{\rm max} = 0.5\,h/{\rm Mpc}$. The contours mark the 68% and 95% confidence intervals. With the redshift-space P_ℓ^g alone, we derive the following 1σ constraints for $\{\Omega_{\rm m}, \Omega_{\rm b}, h, n_s, \sigma_8, M_\nu\}$: **CH:** 0.03443, 0.01219, 0.14069, 0.16552, 0.07701, 0.58119 With the redshift-space B_0^g alone, we get: **CH:** 0.01422, 0.00371, 0.03409, 0.03543, 0.02494, 0.10599. *The galaxy bispectrum substantially improves the constraints on all cosmological parameters over the power spectrum.*

With P_ℓ^g and B_0^g, we derive even better constraints by breaking a number of parameter degeneracies. Among the cosmological parameters, the $\Omega_{\rm m} - \sigma_8$ degeneracy is broken and leads to significant improvements in both $\Omega_{\rm m}$ and σ_8 constraints. Meanwhile, for the HOD parameters, degeneracies

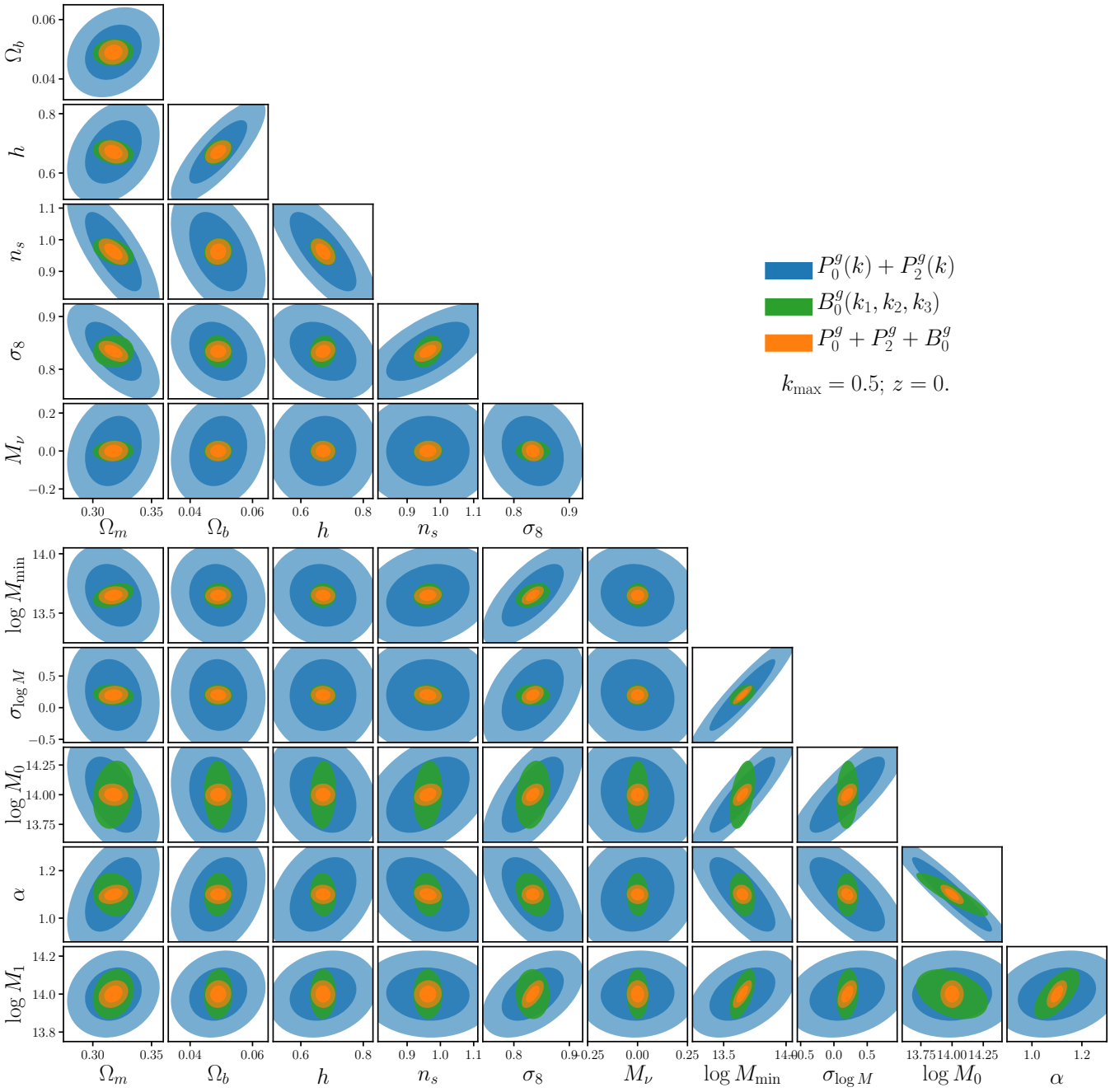

Figure 3. Fisher matrix constraints for M_ν and other cosmological parameters for the redshift-space galaxy P_ℓ^g (blue), B_0^g (green), and combined P_ℓ^g and B_0^g (orange) for $k_{\rm max} = 0.5\,h/{\rm Mpc}$. Our forecasts marginalizes over the Zheng et al. (2007) HOD parameters: $\{M_{\rm min}, \sigma_{\log M}, \log M_0, \alpha \log M_1\}$ (bottom panels). The contours mark the 68% and 95% confidence intervals. The bispectrum substantially improves constraints on all of the cosmological parameters over the power spectrum. $\Omega_{\rm m}$, $\Omega_{\rm b}$, h, n_s, and σ_8 constraints improve by factors of **CH:** 1.9, 2.6, 3.1, 3.6, and 2.6, respectively. For M_ν, the bispectrum improves σ_{M_ν} from **CH:** 0.2968 to 0.0572 eV — over a factor of ~ 5 improvement over the power spectrum.

Table 2. Marginalized Fisher parameter constraints from the redshift-space P_ℓ, B_0, and $P_\ell + B_0$. We list constraints for cosmological parameters M_ν, Ω_m, Ω_b, h, n_s, and σ_8 as well as HOD and nuisance parameters.

	$k_{\rm max} = 0.2$			$k_{\rm max} = 0.5$		
	P_ℓ	B_0	$P_\ell + B_0$	P_ℓ	B_0	$P_\ell + B_0$
M_ν						
$\Omega_{\rm m}$						
$\Omega_{\rm b}$						
h						
n_s						
σ_8						
$M_{\rm min}$						
$\sigma_{\log M}$						
$\log M_0$						
α						
$\log M_1$						

with $\log M_0$, α, and $\log M_1$ are substantially reduced. Combining P_ℓ^g and B_0^g, we get the following 1σ constraints for $\Omega_{\rm m}$, $\Omega_{\rm b}$, h, n_s, σ_8, and M_ν: **CH:** 0.01033, 0.00336, 0.03150, 0.03361, 0.01641, and 0.10299 *With P_ℓ^g and B_0^g combined, we improve $\Omega_{\rm m}$, $\Omega_{\rm b}$, h, n_s, and σ_8 constraints by factors of* **CH:** *3.3, 3.6, 4.5, 4.9, and 4.7 and M_ν constraint by a factor of 5.6.*

In Figure 4, we present the marginalized 1σ constraints, $\sigma_\theta(k_{\rm max})$, of the cosmological parameters $\Omega_{\rm m}$, $\Omega_{\rm b}$, h, n_s, σ_8, and M_ν as a function of $k_{\rm max}$ for P_ℓ^g (blue) and the combined $P_\ell^g + B_0^g$ (orange). Again, these constraints are marginalized over the Zheng et al. (2007) HOD parameters (Eq. 4). For both P_ℓ^g and $P_\ell^g + B_0^g$, parameter constraints improve at higher $k_{\rm max}$. More importantly, *the galaxy bispectrum significantly improves constraints on all cosmological parameters throughout the $k_{\rm max}$ range and not only at high $k_{\rm max}$*. Even for $k_{\rm max} \sim 0.2\,h/{\rm Mpc}$, including B_0^g improves $\Omega_{\rm m}$, $\Omega_{\rm b}$, h, n_s, σ_8 and M_ν constraints by factors of **CH:** 2.6, 2.4, 2.7, 3.2, 4.1, and 3.6.

We also present $\sigma_\theta(k_{\rm max})$ for P_ℓ^g (blue dashed) and $P_\ell^g + B_0^g$ (orange dashed) *with priors from* Planck . Once we include *Planck* priors, P_ℓ^g constraints do not improve for $k_{\rm max} \gtrsim 0.12\,h/{\rm Mpc}$. However, the constraining power of $P_\ell^g + B_0^g$ continues to increase for $k_{\rm max} > 0.15\,h/{\rm Mpc}$. At $k_{\rm max} = 0.2\,h/{\rm Mpc}$, B_0^g improves the P_ℓ^g + *Planck* priors constraints on $\Omega_{\rm m}$, $\Omega_{\rm b}$, h, n_s, σ_8 and M_ν constraint by factors of **CH:** 1.5, 1.4, 1.4, 1.1, 1.3, and 1.4×. At $k_{\rm max} = 0.5\,h/{\rm Mpc}$, B_0^g improves the P_ℓ^g + *Planck* priors constraints on $\Omega_{\rm m}$, $\Omega_{\rm b}$, h, n_s, σ_8 and M_ν constraint by factors of **CH:** 2.1, 2.1, 2.0, 1.2, 2.2, and 2.2× Even with *Planck* priors, the galaxy bispectrum significantly improves cosmological constraints. In fact, we emphasize that the constraints in Figure 4 are for a 1 $({\rm Gpc}/h)^3$ box. Hence, they *underestimate* the constraining power contribution from galaxy clustering that we expect from upcoming galaxy redshift surveys, which will probe a much larger volume (*e.g.* DESI, Euclid). With

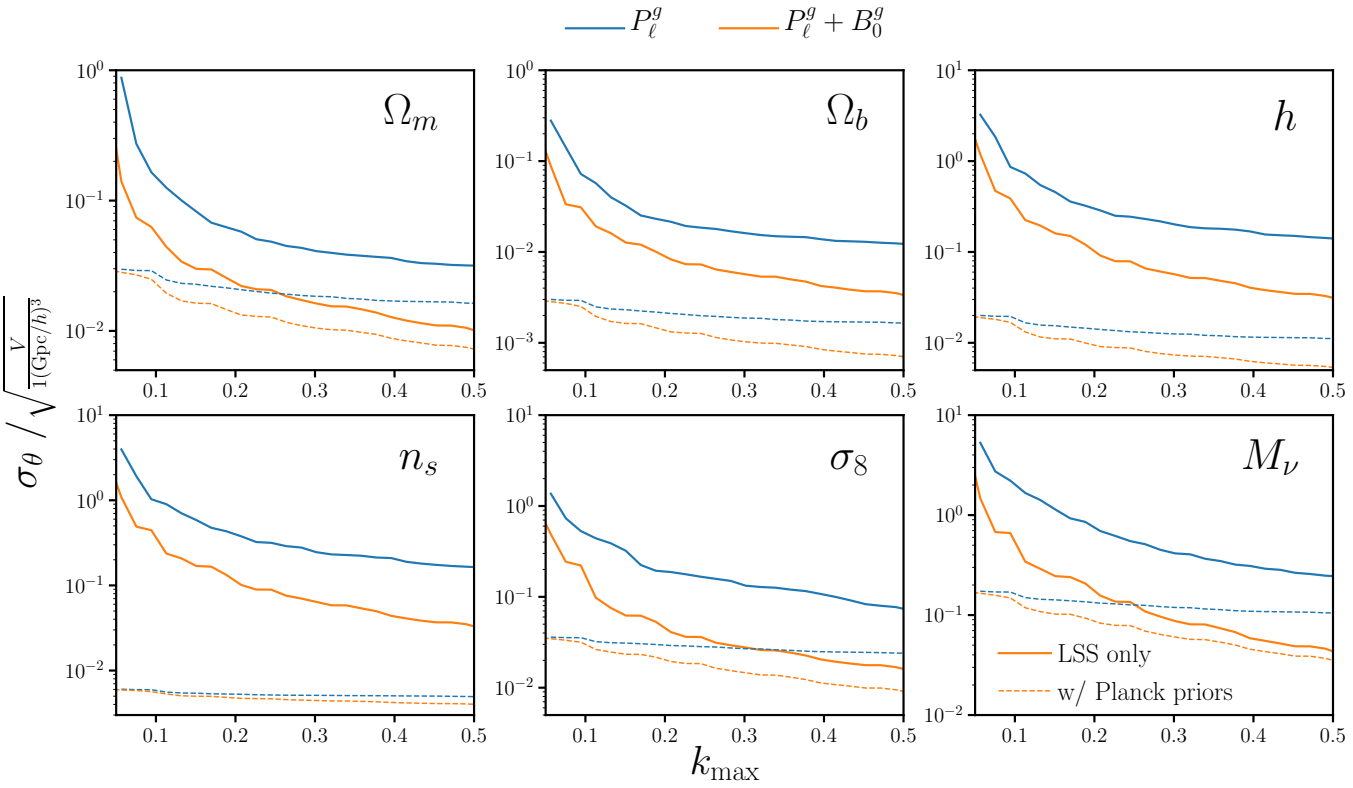

Figure 4. Marginalized 1σ constraints, σ_θ, of the cosmological parameters Ω_m, Ω_b, h, n_s, σ_8, and M_ν as a function of k_max for the redshift-space P_ℓ^g (blue) and combined $P_\ell^g + B_0^g$ (orange). Even after marginalizing over HOD parameters (Eq. 4), the galaxy bispectrum *significantly* improves cosmological parameter constraints above $k_\mathrm{max} > 0.1\,h/\mathrm{Mpc}$. Constraints from P_ℓ^g and $P_\ell^g + B_0^g$ improve with higher k_max. *Throughout* $0.2 < k_\mathrm{max} < 0.5$*, including the bispectrum improves* $\{\Omega_\mathrm{m}, \Omega_\mathrm{b}, h, n_s, \sigma_8, M_\nu\}$ *by* **CH:** *X, Y %*. When we include *Planck* priors (dotted), the improvement from B_0^g is even more evident. The constraining power of P_ℓ^g complete saturates for $k_\mathrm{max} \gtrsim 0.12\,h/\mathrm{Mpc}$. Adding B_0^g not only improves constraints, but the constraints continue to improve for higher k_max. At $k_\mathrm{max} = 0.2$ and $0.5\,h/\mathrm{Mpc}$, the $P_\ell^g + B_0^g$ improves the M_ν constraint by **CH:** X, Y % over P_ℓ^g. We emphasize that the constraints above are for 1 $(\mathrm{Gpc}/h)^3$ box and thus underestimate the constraining power of upcoming galaxy clustering surveys.

more constraining power coming from galaxy clustering, improvements from including B_0^g to P_ℓ^g and *Planck* will be larger.

In the previous paper of the series, Hahn et al. (2020) presents the full information content of the redshift-space halo bispectrum, B_0^h. For B_0^h to $k_\mathrm{max} = 0.5\,h/\mathrm{Mpc}$, Hahn et al. (2020) find 1σ constraints of 0.012, 0.004, 0.04, 0.036, 0.014, and 0.057 for Ω_m, Ω_b, h, n_s, σ_8 and M_ν. In comparison, we find that B_0^g produces comparable constraints for Ω_b, h, and n_s. On the other hand, B_0^g has less constraining power than B_0^h for Ω_m, σ_8, and M_ν. This is the same for $k_\mathrm{max} = 0.2\,h/\mathrm{Mpc}$. When we compare the signal-to-noise ratios (SNR) of B_0^g and B_0^h, estimated from the covariance matrix (*e.g.* Sefusatti & Scoccimarro 2005; Sefusatti et al. 2006; **?**), we find lower SNR for B_0^g, consistent with the constraints. We also find that the increase in SNR with k_max is lessened for

B_0^g. This demonstrates that marginalizing over HOD parameters reduces some of the constraining power of B_0^g. Fingers-of-god (FoG), also contributes to this reduction. **CH:** elaborate on how FoG. Nevertheless, B_0^g significantly improves parameters constraints over P_ℓ^g. In fact, marginalizing over HOD parameters and FoG reduces the constraining power of the power spectrum more so than the bispectrum. Therefore, we find larger improvements in the parameter constraints from B_0^g over P_ℓ^g than from B_0^h over P_ℓ^h.

A number of previous works have quantified the information content of the bispectrum: (*e.g.* Scoccimarro et al. 2004; Sefusatti et al. 2006; Sefusatti & Komatsu 2007; Song et al. 2015; Tellarini et al. 2016; Yamauchi et al. 2017; Karagiannis et al. 2018; Yankelevich & Porciani 2019; Chudaykin & Ivanov 2019; Coulton et al. 2019; Reischke et al. 2019). We, however, focus our comparison to Sefusatti et al. (2006), Yankelevich & Porciani (2019), and Chudaykin & Ivanov (2019), which provide bispectrum forecasts for full sets of cosmological parameters. Sefusatti et al. (2006) present ΛCDMforecasts for a joint likelihood analysis of B_0^g with P^g and WMAP. For $k_{\rm max} = 0.2\,h/{\rm Mpc}$, they find that including B_0^g improves constraints on $\Omega_{\rm m}$, $\Omega_{\rm b}$, h, n_s, and σ_8 by 1.6, 1.2, 1.5, 1.4, and 1.5 times from the P^g and WMAP constraints. In comparison, for $k_{\rm max} = 0.2\,h/{\rm Mpc}$ and with *Planck* priors, we find B_0^g improves constraints by 1.5, 1.4, 1.4, 1.1, and 1.3×, which is in good agreement with Sefusatti et al. (2006). We note, however, that there are some significant differences in our analyses. First, Sefusatti et al. (2006) uses the WMAP likelihood while we use priors from *Planck* . Furthermore, in our simulation-based approach, we marginalizes over the HOD parameters. On the other hand, Sefusatti et al. (2006) use a perturbation theory approach and marginalize over the linear and quadratic bias terms (b_1, b_2). Nevertheless, the improvement Sefusatti et al. (2006) find in parameter constraints including B_0^g is in good agreement with our results.

Next, Yankelevich & Porciani (2019) present ΛCDM, wCDM and w_0w_aCDM Fisher forecasts for a Euclid-like survey**?** over $0.65 < z < 2.05$. Focusing only on their ΛCDMforecasts, they find that for $k_{\rm max} = 0.15\,h/{\rm Mpc}$, $P^g + B_0^g$ produces constraints on $\Omega_{\rm cdm}$, $\Omega_{\rm b}$, A_s, h, n_s that are ∼1.3× tighter than P^g alone. With *Planck* priors, they find parameter constraints improve by a factor of ∼1.1. In contrast, we find even at $k_{\rm max} = 0.15\,h/{\rm Mpc}$ significantly larger improvement in the parameter constraints from including B_0^g. However, we similarly find that the improvement descreases once we include *Planck* priors (Figure 4).

Although Yankelevich & Porciani (2019) find significantly less improvement in parameter constraints from B_0^g, we emphasize that Yankelevich & Porciani (2019) present forecasts for a significantly different galaxy sample — *i.e.* the Euclid survey over $0.65 < z < 2.05$. For instance, their $z = 0.7$ redshift bin has $\bar{n}_g = 2.76 \times 10^{-3}\ h^3{\rm Gpc}^{-3}$ and linear bias of $b_g = 1.18$. Meanwhile our galaxy sample is at $z = 0$ with $\bar{n}_g \sim 1.63 \times 10^{-4}\ h^3{\rm Gpc}^{-3}$ and linear bias of $b_g \sim 2.55$ (Section 3). Furthermore, while we use the HOD framework, they use a bias expansion with linear, non-linear, and tidal bias (b_1, b_2, and b_{s^2}). They also marginalize over 56 nuisance parameters since they jointly analyze 14 z bins, each with 4 nuisance parameters. Lastly, unlike our simulation-based approach, Yankelevich & Porciani (2019) use perturbation theory models and, therefore, limit their forecast to $k_{\rm max} = 0.15\,h/{\rm Mpc}$ due to theoretical uncertainties. Nevertheless, when they estimate the constrain-

ing power beyond $k_{\rm max} > 0.15\,h/{\rm Mpc}$ using Figure of Merit they find that the constraining power of B_0^g relative to P^g increases for higher $k_{\rm max}$ consistent with our results.

Finally, Chudaykin & Ivanov (2019) present M_ν + ΛCDMforecasts for the power spectrum and bispectrum of a Euclid-like survey over $0.5 < z < 2.1$. For $\omega_{\rm cdm}$, ω_b, h, n_s, A_s, and M_ν they find $\sim$1.2, 1.5, 1.4, 1.3, and 1.1$\times$ tighter constraints from P_ℓ^g and B_0^g than from P_ℓ^g alone. For M_ν, they find a factor of 1.4 improvement, from 0.038 eV to 0.028 eV. With *Planck* , they get $\sim$2, 1.1, 2.3, 1.5, 1.1, and 1.3$\times$ tighter constraints for $\omega_{\rm cdm}$, ω_b, h, n_s, A_s, and M_ν from including B_0^g. Overall, Chudaykin & Ivanov (2019) find significant improvements from including B_0^g — consistent with our results. However, they find more modest improvements than we find in Figures 3 and 4.

Again, there are significant differences between our anlayses. First, like Yankelevich & Porciani (2019), Chudaykin & Ivanov (2019) present forecasts for a Euclid-like survey, which is significantly different than our galaxy sample. Their $z = 0.6$ redshift bin, for instance, has $\bar{n}_g = 3.83 \times 10^{-3}\ h^3{\rm Gpc}^{-3}$ and linear bias of $b_g = 1.14$. Next, they include the Alcock-Paczynski (AP) effect for P_ℓ^g but not for B_0^g. They find that including the AP effect significantly improves P_ℓ^g constraints (e.g. tightens M_ν constraints by $\sim$30%); this reduces the improvement they report from including B_0^g.

Another difference between our analyses is that although Chudaykin & Ivanov (2019) use a more accurate Markov-Chain Monte-Carlo (MCMC) approach to derive parameter constraints, they neglect the non-Gaussian contributions to both P_ℓ^g and B_0^g covariance matrices and also do not include the covariance between P_ℓ^g and B_0^g for the joint constraints. We find that neglecting the covariance between P_ℓ^g and B_0^g overestimates constraints by **CH:** XXXX for our $k_{\rm max} = 0.2\,h/{\rm Mpc}$ constraints. Lastly, Chudaykin & Ivanov (2019) use a one-loop and tree-level perturbation theory to model P_ℓ^g and B_0^g, respectively. Rather than imposing a $k_{\rm max}$ cutoff to restrict their forecasts to scales where their perturbation theory models can be trusted, they use a theoretical error covariance model approach from **?**. With a tree-level B_0^g model, theoretical errors quickly dominate at $k_{\rm max} \gtrsim 0.1\,h/{\rm Mpc}$, where one- and two-loop contribute significantly (*e.g.* Lazanu & Liguori 2018). So effectively, their forecasts do not include the constraining power on those scales. In fact, if we restrict our forecast to $k_{\rm max} = 0.25\,h/{\rm Mpc}$ for P_ℓ^g and $k_{\rm max} = 0.1\,h/{\rm Mpc}$ for B_0^g, our $\Omega_{\rm m}$, $\Omega_{\rm b}$, h, n_s, σ_8, and M_ν constraints improve by 1.3, 1.2, 1.2, 1.4, 2.0, and 1.7$\times$ from including B_0^g, roughly consistent with Chudaykin & Ivanov (2019).

Among the various differences between our forecast and previous works, we emphasize that we use a simulationed-based approach. This, combined with the immense number of simulations, is what allows us to go beyond previous perturbation theory approaches and accurately quantify the constraining power in the nonlinear regime. Furthermore, this allows us to derive, for the first time, the total information content of the redshift-space galaxy power spectrum and bispectrum down to nonlinear scales and demonstrate the constraining power of the galaxy bispectrum for M_ν.

A simulation-based approach, however, has a few caveats, which we discuss below. First, our forecasts rely on the stability and convergence of the covariance matrix and numerical derivatives. For our constraints we use 195000 galaxy catalogs (Section 3): 15,000 for the covariance matrices and 180,000 for the derivatives with respect to 11 parameters. To ensure that our results are robust, we conduct the same set of convergence tests as Hahn et al. (2020). First, we test whether our results

have sufficiently converged by deriving our constraints using different numbers of galaxy catalogs to estimate the covariance matrix and derivatives: $N_{\rm cov}$ and $N_{\rm deriv}$. For $N_{\rm cov}$, we find $< XXXX\%$ variation σ_θ for $N_{\rm cov} > 12000$. For $N_{\rm deriv}$, we find $< XXXX\%$ variation σ_θ for $N_{\rm cov} > 12000$. vary by $< 10\%$, we conclude that the conergence of the covariance matrix or deriviatves do not significantly impact our forecast. **CH:** fill this in once we have the convergence test.

Besides the convergence of the numerical derivatives, the M_ν derivatives can be evaluated using different sets of cosmologies. In our anlaysis, we evaluate $\partial P_\ell^g/\partial M_\nu$ and $\partial B_0^g/\partial M_\nu$ using simulations at the $\{\theta_{\rm ZA}, M_\nu^+, M_\nu^{++}, M_\nu^{+++}\}$ cosmologies. They can, however, also be estimated using two other sets of cosmologies: (i) $\{\theta_{\rm ZA}, M_\nu^+\}$ and (ii) $\{\theta_{\rm ZA}, M_\nu^+, M_\nu^{++}\}$. If we used (i) estimates for $\partial P_\ell^g/\partial M_\nu$ and $\partial B_0^g/\partial M_\nu$, compared to our forecasts, we get **CH:** XXXXX. For (ii), we get **CH:** XXXX. **CH:** check this once the multiple HOD seeds finish.

For our fiducial HOD paramters other than $\sigma_{\log M}$, we chose values based on Zheng et al. (2007) fits to the SDSS $M_r < -21.5$ and -22 samples (Section 3). For $\sigma_{\log M}$, due to the halo mass limit of Quijote, we chose a tighter scatter of 0.2 dex. As a result, our HOD galaxy catalogs have a different selection function than observed samples, which are yptically based on M_r or M_* cuts (*e.g.* SDSS or BOSS). To test the impact of the fiducial $\sigma_{\log M}$ choice, **CH:** in Appendix **??**, we compare $\partial P_\ell^g/\partial \sigma_{\log M}$ and $\partial B_0^g/\partial \sigma_{\log M}$ at $\sigma_{\log M} = 0.2$ dex to the derivates evaluated at $\sigma_{\log M} =$, estimated using higher resolution Quijote simulations. Fill in after we do the comparison. **CH:** what can we say about the sigma8-sigmalogM degeneracy?

Besides their convergence and stability, our forecasts are derived from Fisher matrices. We, therefore, assume that the posterior is approximately Gaussian. When posteriors are highly non-elliptical or asymmetric, Fisher forecasts significantly underestimate the constraints (Wolz et al. 2012). We note that in this paper we do not derive actual parameter constraints. Instead, we focus on quantifying the information content and constraining power of B_0^g relative to P_ℓ^g. Hence, we do not explore beyond the Fisher forecast. In a later paper of the series, when we analyze the SDSS-III BOSS data using a simulation-based approach, we will use a robust method to sample the posterior.

Besides the caveats above, a number of extra steps and complications remain between this work and a full galaxy bispectrum analysis using a simulationed based approach. For instance, we use the basic Zheng et al. (2007) HOD model, which does not include assembly bias. Zentner et al. (2016) and Vakili & Hahn (2019) find little evidence for assembly bias in the galaxy clustering of the SDSS $M_r < -21.5$ and -21 samples. Beltz-Mohrmann et al. (2020) also found that the basic HOD is sufficent to reproduce several galaxy clustering statistics (*e.g.* projected 2PCF, 2PCF, group multiplicity function) of high luminosity galaxies in the Illustris and EAGLE hydrodynamic simulations. While the basic HOD is likely sufficient for the forecast we present, many works have demonstrated that assembly bias impacts galaxy clustering for lower luminsoity/mass samples both using observations (**????**Vakili & Hahn 2019; **?**) and hydrodynamic simulations (Chaves-Montero et al. 2016; Beltz-Mohrmann et al. 2020).

In addition to assembly bias, central and satellite velocity biases can also impact galaxy clustering (Guo et al. 2015b,a). Central galaxies, in both observations and simulations, are not at rest in the centers of the host halos (*e.g.* **????**). Similarly, satellite galaxies in simulations do not have the

same velocities as the underlying dark matter (*e.g.* **??????**). This velocity bias in centrals reduces the Kaiser effect; while in satellites, it reduces the FoG effect. For the high luminosity SDSS samples, Guo et al. (2015a) find little satellite velocity bias. While they find some central velocity bias, their constraints are based on galaxy clustering on very small scales ($\sim 0.1 - 25 h^{-1}$Mpc). More recently, **?** found that removing central and satellite velocity biases for the Illustris and EAGLE simulations had little impact on various clustering measurements of their high luminosity sample. Although assembly bias and velocity bias do not likely impact the forecasts we present, for lower luminosity/mass galaxy samples and for higher precision measurements of observations they must be included. The improvements we see in HOD parameter constraints from B_0^g in Figure 3 suggest that B_0^g also has the potential to better constrain the assembly bias parameters and improve our understanding of the galaxy-halo connection. Therefore, when we analyze observations with a simulation-based approach later in the series, we will use a decorated HOD framework (such as *e.g.* Vakili & Hahn 2019; Zhai et al. 2019, **CH:** others) that includes both assembly bias and velocity biases.

Our analysis also does not include baryonic effects. Although they have been typically neglected in galaxy clustering analyses, baryonic effects, such as feedback from active galactic nuclei (AGN), can impact the matter distribution at cosmological distances (*e.g.* **????**Harnois-Déraps et al. 2015). For AGN feedback in particular, various works have an impact on the matter power spectrum (*e.g.* **??????**van Daalen et al. 2020). Although there is no consensus on the magnitude of the effect, ultimately, a more effective AGN feedback increases the impact on the matter clustering (Barreira et al. 2019). In state-of-the-art hydrodynamical simulations (TNG, EAGLE, and BAHAMAS), Foreman et al. (2019) find $\lesssim 1\%$ impact on the matter power spectrum at $k \lesssim 0.5\, h$/Mpc. For the matter bispectrum, Foreman et al. (2019) find that the effect of baryons is peaked at $k = 3\, h$/Mpc and, similarly, a $\lesssim 1\%$ effect at $k \lesssim 0.5\, h$/Mpc. Despite the growing evidence of baryon impacting the matter clustering, the effect is mainly seen on scales smaller than what is probed by galaxy clustering analyses with spectroscopic redshift surveys. We, therefore, do not include baryonic effects in our forecasts and do not consider it further in the series.

In our forecasts, we use B_0^g with triange defined in k_1, k_2, k_3 bins of width $\Delta k = 3k_f = 0.01885\, h$/Mpc (Section 4). Gagrani & Samushia (2017) find that for the growth rate parameter bispectrum multipoles beyond the monopole have significant constraining power. Yankelevich & Porciani (2019), with figure-of-merit (FoM) estimates, also find significant information content beyond the monopole. Furthermore, Yankelevich & Porciani (2019) also find that coarser binning of the triangle configurations reduces the information content of the bispectrum. Binning by $\Delta k = 3k_f$ has $\sim 10\%$ less constraining power than binning by $\Delta k = k_f$. Including higher order multipoles and increase the binning are both straightforward to implement; however, they both increase the dimensionality of the data vector. B_0^g alone binned by $\Delta k = 3k_f$ already has 1898 dimensions. Hence, including multipoles and increasing the binning is not feasible for a full bispectrum analysis without the use of data compression (*e.g.* Byun et al. 2017; Gualdi et al. 2018, 2019b,a). For future papers in the series, we will include bispectrum multipoles and finer binning in conjunction with data compression.

Lastly, our forecasts are derived using periodic boxes and do not consider a realistic geometry or radial selection function of galaxy surveys. A realistic selection function will smooth the trian-

gle configuration dependence and degrade the constraining power of the bispectrum (Sefusatti & Scoccimarro 2005). We also do not account for super-sample covariance, which may also impact our constraints (Hamilton et al. 2006; Sefusatti et al. 2006; Takada & Hu 2013; Li et al. 2018; Wadekar & Scoccimarro 2019). Since these effects also affect the power spectrum, we expect to find substantial improvements in cosmological parameter constraints from including the bispectrum, especially for M_ν.

In this paper, we present the total information content and constraining power of the galaxy bispectrum down to the nonlinear regime. Even after marginalizing over galaxy bias, through the HOD parameters, including B_0^g provides substantial improvements in cosmological parameter constraints — especially M_ν. A combined analysis of P_ℓ^g and B_0^g breaks several key parameter degeneracies that limit an analysis of P_ℓ^g alone. We find that the significant improvements from B_0^g even at $k_{\rm max} \sim 0.2\,h/{\rm Mpc}$ and with *Planck* priors. Furthermore, we emphasize that the constraints we present is for a $1h^{-1}{\rm Gpc}$ box and $\bar{n}_g \sim 1.63 \times 10^{-4}\ h^3{\rm Gpc}^{-3}$. Upcoming surveys will probe substantially larger cosmic volumes with higher number densities. We discuss a number of factors that will impact the constraining power of B_0^g for actual galaxy clustering analyses, such as assembly bias, survey geometry, super-sample covariance, and etc. Even if the constraining power is reduced, our forecasts suggest that the galaxy bispectrum will significantly improve cosmology parameter constraints.

Now that we have demonstrated the constraining power of B_0^g, in the following paper of this series we will address a major practical challenge for a B_0^g analysis — its large dimensionality. We will present how data compression can be used to reduce the dimensionality and tractably estimate the covariance matrix in a P_ℓ^g and B_0^g analysis using a simulation-based approach. Afterwards, the series will culminate in fully simulation-based P_ℓ^g and B_0^g reanalysis of SDSS-III BOSS.

6. SUMMARY

Afterwards, we will apply it to future surveys. **CH:** rough numbers of DESI, PFS, and Euclid

ACKNOWLEDGEMENTS

It's a pleasure to thank Mehmet Alpaslan, Arka Banerjee, Joseph DeRose, Daniel Eisenstein, Mikhail Ivanov, Elena Massara, Jeremy L. Tinker, Roman Scoccimarro, Uroš Seljak, Zachary Slepian, Digvijay Wadekar, Risa Wechsler ... for valuable discussions and comments.

APPENDIX

REFERENCES

Alpaslan, M., & Tinker, J. L. 2019, arXiv e-prints, 1911, arXiv:1911.04509

Barreira, A., Nelson, D., Pillepich, A., et al. 2019, Monthly Notices of the Royal Astronomical Society, 488, 2079

Beltz-Mohrmann, G. D., Berlind, A. A., & Szewciw, A. O. 2020, Monthly Notices of the Royal Astronomical Society, 491, 5771

Beutler, F., Seo, H.-J., Saito, S., et al. 2017, Monthly Notices of the Royal Astronomical Society, 466, 2242

Brandbyge, J., Hannestad, S., Haugbø lle, T., & Thomsen, B. 2008, Journal of Cosmology and Astro-Particle Physics, 08, 020
Byun, J., Eggemeier, A., Regan, D., Seery, D., & Smith, R. E. 2017, Monthly Notices of the Royal Astronomical Society, 471, 1581
Carron, J. 2013, Astronomy & Astrophysics, 551, A88
Chaves-Montero, J., Angulo, R. E., Schaye, J., et al. 2016, Monthly Notices of the Royal Astronomical Society, 460, 3100
Chudaykin, A., & Ivanov, M. M. 2019, arXiv:1907.06666 [astro-ph, physics:hep-ph], arXiv:1907.06666 [astro-ph, physics:hep-ph]
Contreras, S., Angulo, R., & Zennaro, M. 2020, arXiv e-prints, 2005, arXiv:2005.03672
Coulton, W. R., Liu, J., Madhavacheril, M. S., Böhm, V., & Spergel, D. N. 2019, Journal of Cosmology and Astro-Particle Physics, 2019, 043
Dalal, N., Doré, O., Huterer, D., & Shirokov, A. 2008, Physical Review D, 77, arXiv:0710.4560
Davis, M., Efstathiou, G., Frenk, C. S., & White, S. D. M. 1985, The Astrophysical Journal, 292, 371
Dodelson, S. 2003, Modern Cosmology
Foreman, S., Coulton, W., Villaescusa-Navarro, F., & Barreira, A. 2019, arXiv e-prints, 1910, arXiv:1910.03597
Gagrani, P., & Samushia, L. 2017, Monthly Notices of the Royal Astronomical Society, 467, 928
Gao, L., Springel, V., & White, S. D. M. 2005, Monthly Notices of the Royal Astronomical Society, 363, L66
Gualdi, D., Gil-Marín, H., Manera, M., Joachimi, B., & Lahav, O. 2019a, Monthly Notices of the Royal Astronomical Society: Letters, arXiv:1901.00987
Gualdi, D., Gil-Marín, H., Schuhmann, R. L., et al. 2019b, Monthly Notices of the Royal Astronomical Society, 484, 3713
Gualdi, D., Manera, M., Joachimi, B., & Lahav, O. 2018, Monthly Notices of the Royal Astronomical Society, 476, 4045
Guo, H., Zheng, Z., Zehavi, I., et al. 2015a, Monthly Notices of the Royal Astronomical Society, 453, 4368
—. 2015b, Monthly Notices of the Royal Astronomical Society, 446, 578
Hadzhiyska, B., Bose, S., Eisenstein, D., Hernquist, L., & Spergel, D. N. 2020, Monthly Notices of the Royal Astronomical Society, 493, 5506
Hahn, C., Villaescusa-Navarro, F., Castorina, E., & Scoccimarro, R. 2020, Journal of Cosmology and Astroparticle Physics, 03, 040
Hamilton, A. J. S., Rimes, C. D., & Scoccimarro, R. 2006, Monthly Notices of the Royal Astronomical Society, 371, 1188
Harker, G., Cole, S., Helly, J., Frenk, C., & Jenkins, A. 2006, Monthly Notices of the Royal Astronomical Society, 367, 1039
Harnois-Déraps, J., van Waerbeke, L., Viola, M., & Heymans, C. 2015, Monthly Notices of the Royal Astronomical Society, 450, 1212
Heavens, A. 2009, arXiv:0906.0664 [astro-ph], arXiv:0906.0664 [astro-ph]
Hockney, R. W., & Eastwood, J. W. 1981, Computer Simulation Using Particles
Jungman, G., Kamionkowski, M., Kosowsky, A., & Spergel, D. N. 1996, Physical Review D, 54, 1332
Karagiannis, D., Lazanu, A., Liguori, M., et al. 2018, Monthly Notices of the Royal Astronomical Society, 478, 1341
Lacerna, I., Padilla, N., & Stasyszyn, F. 2014, Monthly Notices of the Royal Astronomical Society, 443, 3107
Lazanu, A., & Liguori, M. 2018, Journal of Cosmology and Astro-Particle Physics, 2018, 055
Leauthaud, A., Tinker, J., Bundy, K., et al. 2012, The Astrophysical Journal, 744, 159
Li, Y., Schmittfull, M., & Seljak, U. 2018, Journal of Cosmology and Astro-Particle Physics, 2018, 022
McClintock, T., Rozo, E., Becker, M. R., et al. 2018, arXiv:1804.05866 [astro-ph], arXiv:1804.05866 [astro-ph]
Navarro, J. F., Frenk, C. S., & White, S. D. M. 1997, The Astrophysical Journal, 490, 493
Reischke, R., Desjacques, V., & Zaroubi, S. 2019, arXiv:1909.03761 [astro-ph], arXiv:1909.03761 [astro-ph]
Rodríguez-Torres, S. A., Chuang, C.-H., Prada, F., et al. 2016, Monthly Notices of the Royal Astronomical Society, 460, 1173

Rodríguez-Torres, S. A., Comparat, J., Prada, F., et al. 2017, Monthly Notices of the Royal Astronomical Society, 468, 728
Scoccimarro, R. 2015, Physical Review D, 92, arXiv:1506.02729
Scoccimarro, R., Sefusatti, E., & Zaldarriaga, M. 2004, Physical Review D, 69, 103513
Sefusatti, E., Crocce, M., Pueblas, S., & Scoccimarro, R. 2006, Physical Review D, 74, arXiv:astro-ph/0604505
Sefusatti, E., Crocce, M., Scoccimarro, R., & Couchman, H. M. P. 2016, Monthly Notices of the Royal Astronomical Society, 460, 3624
Sefusatti, E., & Komatsu, E. 2007, Physical Review D, 76, 083004
Sefusatti, E., & Scoccimarro, R. 2005, Physical Review D, 71, arXiv:astro-ph/0412626
Sheth, R. K., & Tormen, G. 2004, Monthly Notices of the Royal Astronomical Society, 350, 1385
Sinha, M., Berlind, A. A., McBride, C. K., et al. 2018, Monthly Notices of the Royal Astronomical Society, 478, 1042
Song, Y.-S., Taruya, A., & Oka, A. 2015, Journal of Cosmology and Astro-Particle Physics, 2015, 007
Springel, V. 2005, Monthly Notices of the Royal Astronomical Society, 364, 1105
Takada, M., & Hu, W. 2013, Physical Review D, 87, 123504
Tegmark, M., Taylor, A. N., & Heavens, A. F. 1997, The Astrophysical Journal, 480, 22
Tellarini, M., Ross, A. J., Tasinato, G., & Wands, D. 2016, Journal of Cosmology and Astro-Particle Physics, 2016, 014
Tinker, J. L., Leauthaud, A., Bundy, K., et al. 2013, The Astrophysical Journal, 778, 93
Vakili, M., & Hahn, C. 2019, The Astrophysical Journal, 872, 115
van Daalen, M. P., McCarthy, I. G., & Schaye, J. 2020, Monthly Notices of the Royal Astronomical Society, 491, 2424
Verde, L. 2010, arXiv:0911.3105 [astro-ph], 800, 147
Viel, M., Haehnelt, M. G., & Springel, V. 2010, Journal of Cosmology and Astro-Particle Physics, 06, 015
Villaescusa-Navarro, F., Hahn, C., Massara, E., et al. 2019, arXiv:1909.05273 [astro-ph], arXiv:1909.05273 [astro-ph]
Wadekar, D., & Scoccimarro, R. 2019, arXiv e-prints, 1910, arXiv:1910.02914
Wang, H., Mo, H. J., & Jing, Y. P. 2009, Monthly Notices of the Royal Astronomical Society, 396, 2249
Wechsler, R. H., Zentner, A. R., Bullock, J. S., Kravtsov, A. V., & Allgood, B. 2006, The Astrophysical Journal, 652, 71
Wolz, L., Kilbinger, M., Weller, J., & Giannantonio, T. 2012, Journal of Cosmology and Astroparticle Physics, 2012, 009
Yamauchi, D., Yokoyama, S., & Takahashi, K. 2017, Physical Review D, 95, 063530
Yankelevich, V., & Porciani, C. 2019, Monthly Notices of the Royal Astronomical Society, 483, 2078
Zennaro, M., Bel, J., Villaescusa-Navarro, F., et al. 2017, Monthly Notices of the Royal Astronomical Society, 466, 3244
Zentner, A. R., Hearin, A., van den Bosch, F. C., Lange, J. U., & Villarreal, A. 2016, arXiv:1606.07817 [astro-ph], arXiv:1606.07817 [astro-ph]
Zhai, Z., Tinker, J. L., Becker, M. R., et al. 2019, The Astrophysical Journal, 874, 95
Zheng, Z., Coil, A. L., & Zehavi, I. 2007, The Astrophysical Journal, 667, 760
Zheng, Z., Berlind, A. A., Weinberg, D. H., et al. 2005, The Astrophysical Journal, 633, 791